

Formation of a Coherent Mode in a Double Quantum Dot

R. H. Blick,* D. Pfannkuche, R. J. Haug,† K. v. Klitzing, and K. Eberl

Max-Planck-Institut für Festkörperforschung, Heisenbergstrasse 1, 70569 Stuttgart, Germany

(Received 28 July 1997)

A double quantum dot is investigated in the few electron limit. The dots are coupled by a tunneling barrier allowing the exchange of a “valence” electron, leading to the formation of a *molecular state*. The existence of this molecular state is verified by the determination of the tunnel splitting. [S0031-9007(98)06053-0]

PACS numbers: 73.40.Gk, 73.20.Dx

Single quantum dots, often referred to as “artificial atoms,” have attracted broad interest. Electronic transport through these systems is governed by the mechanism of Coulomb blockade (CB) and single electron tunneling [1]. By coupling two quantum dots in a series, a double quantum dot is formed. This system gains new quality compared to single quantum dots as electrons can be shared between the two sites, thus forming an artificial molecule [2]. Recent experimental approaches mainly addressed the ground state properties of the double quantum dot [3]. Detailed calculations were then given, introducing the model of an “artificial molecule” and its implications for the experiment, especially as Klimeck *et al.* pointed out the importance of the tunnel splitting for measurements [4].

In this Letter we present measurements on such an artificial molecule. The two dots are set up in a lateral geometry and are connected in a series, coupled by a tunneling barrier, thus allowing electrostatic interaction and a finite coupling of the wave functions of the two systems. The two-dimensional electron gas (2DEG) used in this experiment forms in an $\text{Al}_x\text{Ga}_{1-x}\text{As}/\text{GaAs}$ heterostructure grown by molecular beam epitaxy—located 90 nm below the evaporated Schottky gates. The carrier density at a temperature of 4.2 K is $2.05 \times 10^{11} \text{ m}^{-2}$ with a mobility of $80 \text{ m}^2/\text{Vs}$. A Hall-bar structure is etched into the substrate and Ohmic contacts are fabricated. The quantum dots in our experiments are realized by electron-beam written split gates on top of the heterostructure. The conductivity is measured within the common lock-in and preamplifier setup in a dilution refrigerator at a base temperature of 25 mK. The excitation voltage applied has an amplitude of $5 \mu\text{V}$ at a frequency of 14 Hz.

In biasing the split gates on top of the heterostructure, two quantum dots of different sizes are formed. The different sizes are supported by different potentials at the gates and the specific geometry of the gates. The small dot will be termed *A* and the large one *B*. In a detailed numerical study of the electrostatic potential induced by the gate voltages [6], we found good agreement in comparing the calculated dot sizes and the experimentally determined capacities. The absolute number of electrons in dot *A* and *B* obtained from these calculations is $N_A \approx 12 \pm 2$ and $N_B \approx 33 \pm 2$, which agrees with the

capacitance ratio between the two dots of $C_\Sigma^A/C_\Sigma^B \approx \frac{1}{3}$. The charging energies for the two dots evaluate to $E_C^A \cong 3 \text{ meV}$ and $E_C^B = (0.9 \pm 0.11) \text{ meV}$. These are obtained by measuring the drain-source dependence of the CB regime of the two dots [7]. In addition, a back gate (V_{BG}), situated 0.5 mm below the 2DEG, is operated to shift the electrostatic potentials of the two quantum dots.

The double quantum dot is best characterized by measuring its charging diagram, i.e., by varying the electrostatic potentials of two independent gates, while the conductance through the dot system is traced. In our case we varied a top gate and stepped the back gate voltage in increments of 0.5 V, as shown in Fig. 1. The coupling of the dots to the leads, as well as the interdot tunneling barrier, was adjusted to be well into the regime of tunneling. As seen in the gray scale plot, the conductance resonances form a hexagonal lattice with different slopes, according to the different electrostatic coupling between the gates and the dots. The distance between adjacent (parallel) resonance lines reflects the different charging energies of the large (*B*) and the small quantum dot (*A*) ($\delta V_{\text{BG}}^B, \delta V_{\text{BG}}^A$, where BG indicates the back gate). The hexagons are stretched, since the total capacities of the two dots differed strongly.

Since the dots are connected, the charging of one dot influences the electrostatic potential of the other one, which leads to a repulsion of the resonance lines close to the points where the resonances of both dots intersect and, hence, form a hexagon lattice [3]. This displacement is proportional to the interdot capacity C_{id} , as indicated in the schematic charging diagram of Fig. 1(b). An increase in the value of C_{id} lifts the degeneracy of the crossing points. While this formation of a hexagonal lattice in Fig. 2(a), reflecting the regions of stability for a given charge distribution (N_A, N_B), is already well known for coupled metallic islands, we find—in contrast to those systems—a finite conductance far away from the triple points of the charging diagram [see Fig. 1(a)]. Keeping in mind that only at the triple points the conductance resonances of both dots coincide, a finite conductance all along the boundaries of the charging diagram implies that we can—far away from the points of degeneracy—*detune* the resonance condition considerably and still measure transconductance.

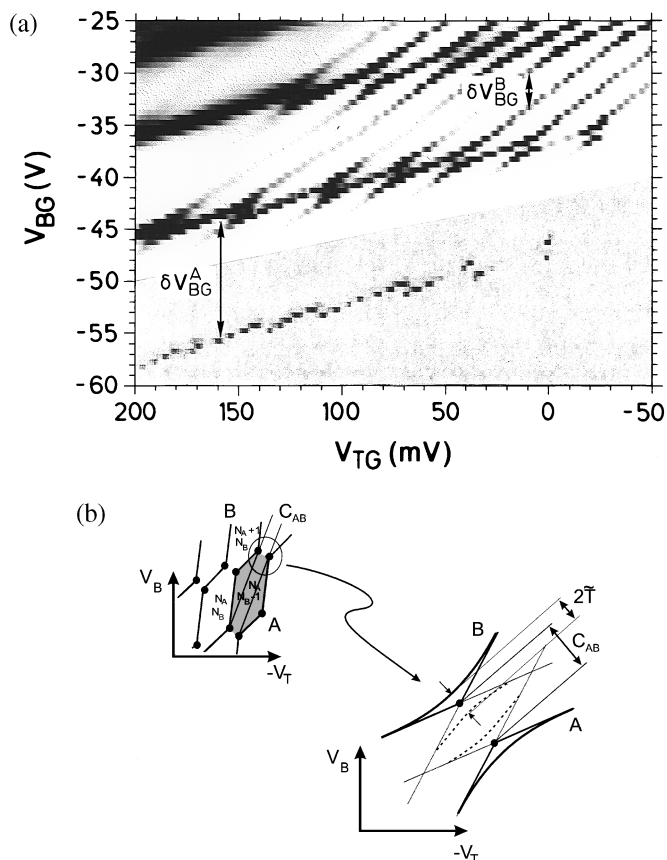


FIG. 1. (a) Measured charging diagrams of the double quantum dot: The TG and BG voltages define the diagram axis, while the different hexagons represent separate charging states with a discrete number of electrons (N_A, N_B). The gray scale minimum is at $\sigma_{\min} = 0 \mu\text{S}$ and the maximum at $\sigma_{\max} = 2.5 \mu\text{S}$. (b) Theoretical charging diagram with a nonzero interdot capacitance C_{id} , resulting in the hexagon lattice. The black dots indicate—for serial coupling—the positions of conductance resonances. The magnified lower part, where different resonance lines are crossing, shows the influence of the tunnel splitting onto the charging diagram: The electrostatic interaction C_{id} determines mainly the splitting at the two resonance points as shown. In addition, the interdot tunnel coupling leads to an enhanced splitting on the order of $2\tilde{T}$.

This observation can be explained by a finite overlap between the wave functions of electrons located in the different dots, even if the corresponding energies are different. The total number of electrons in the double quantum dot does not change when traversing the line connecting two displaced triple points, like, e.g., in the transition $N_A, N_B + 1 \rightarrow N_A + 1, N_B$ where simply an electron moves from dot B to dot A . In this region the “topmost” electron is not localized in one of both dots, but the particle’s wave function is distributed across the whole double dot. This spread out wave function characterizes a *valence electron*. Because of tunneling, the energy of the valence electron is lowered compared to localized electrons [2]. We find a Lorentzian shaped variation of

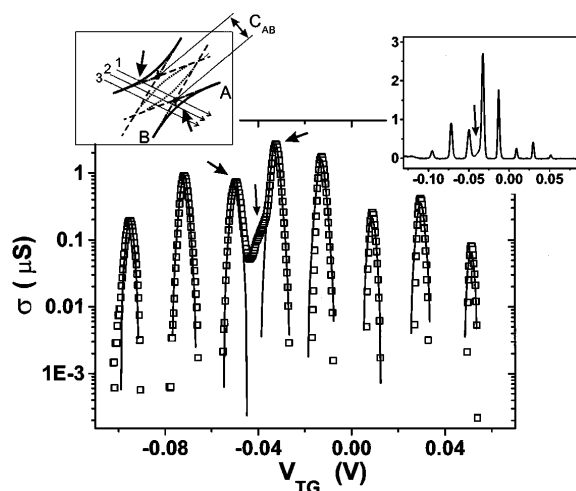


FIG. 2. Measured differential conductance (open boxes) through the double quantum dot and fit according to the derivative of the Fermi-Dirac function $\delta f_{FD}/\delta E$ (solid line) in logarithmic representation. The curve is trace No. 1 out of the charging diagram as depicted in the upper left inset (traces No. 2 and No. 3 are then given in the following figures). The inset schematically shows the crossing point as defined in Fig. 1. The right inset shows the conductance for comparison in linear representation.

the conductance amplitudes due to this molecular binding (data not shown here).

Here we want to focus on the effect of the tunnel splitting which occurs when the two discrete states ϵ_A and ϵ_B overlap forming a valence state. The magnified lower part in Fig. 1(b), where different resonance lines are crossing, shows the influence of the tunnel splitting onto the charging diagram: The electrostatic interaction C_{id} determines mainly the splitting at the two resonance points as shown. In addition, the interdot tunnel coupling \tilde{T} leads to an enhanced splitting on the order of $2\tilde{T}$. Hence, there are four states available for transport. The rounded solid lines mark the ground or symmetric states, while the dashed lines indicate the antisymmetric states [8]. These antisymmetric states can be monitored at selected traces in the charging diagram, as will be shown below.

In Fig. 2 a conductance resonance is shown in logarithmic representation corresponding to a horizontal line through the charging diagram in Fig. 1(a) ($V_{BG} = -38.5 \text{ V}$). The open boxes are the measured conductance values, and the solid line corresponds to a fit according to the derivative of the Fermi-Dirac function at an electron temperature of 100 mK. For comparison, the upper right inset shows the same trace in a linear representation. Obviously we find at the crossing point of the resonance lines—marked by the arrow in the center—a strong asymmetry of the conductance peak structure, which cannot be fitted. This asymmetry is well pronounced in the log plot, while the peaks to the left and right (arrows) reveal symmetric flanks. As a reminder, the upper left

inset shows the magnified part of the charging diagram in the previous figure. The curve in the log plot corresponds to trace No. 1, as indicated in the inset—it crosses the left ground state and then the two states on the right side, which are the anti- and the symmetric states. Hence, the shoulder in the right conductance peak—the *tunnel splitted state*—is formed.

To confirm this picture we chose different traces from the charging diagram crossing the region of interest at different points. The traces are indicated in the upper left inset of Fig. 2. These are labeled No. 1, No. 2, and No. 3 and correspond to variations in the coupling of the discrete states. The beauty of this method is the possibility to simply measure the whole diagram and afterwards being able to extract the conductance resonance trace.

The data obtained are given in Figs. 3 and 4: We focus on the two main peaks in the center of the conductance traces—the data are plotted on a logarithmic scale again. In Fig. 3(a) the resonance of Fig. 2 is shown, clearly the asymmetry and thus the inefficient fitting by a single resonance is found. This is caused by the tunnel splitted state, which contributes to transport through the coupled system (see Fig. 1). In detuning the back gate voltage to -38 V, we observe a diminishing of the conductance found in the shoulder of the right peak, as shown in Fig. 3(b). Hence, the coupling strength switched, and we

find the ground state resonances contributing to transport. The double dot is detuned in this case.

In Fig. 4 the conductance resonances are shown when the back gate is tuned in the opposite direction compared to Fig. 3 to -39 and -39.5 V—these traces refer to the sequentially numbered cuts No. 2 and No. 3. In accordance with these traces we find in Fig. 4(a) that the additional resonance structure now moved from the right peak's shoulder into the left one. Hence, the tunnel splitted resonance of the left peak now contributes to the overall conductance. Moreover, we can state that the amplitudes of two tunnel splitted states switched. This switching indicates the symmetry of the whole process. Under further detuning we observe that this tunnel splitting is damped out, and merely a background conductance remains.

From these measurements and data from other crossing points we determine the tunnel splitting to be on the order of $\delta\epsilon \cong 120 \mu\text{eV}$. This value excludes an interpretation of the additional resonance as an excited dot state, since the excitation energies in quantum dot *A* are found to be much higher, on the order of $400 \mu\text{eV}$.

For comparison we show in Fig. 5 a resonance peak farther away from the crossing point, where the tunnel splitting is negligible. The curve is fitted as before with the derivative of the Fermi-Dirac function and clearly follows. The left tail shows a slight deviation; this side of the peak is directed towards the crossing point. We conclude that this nonzero conductance far away from

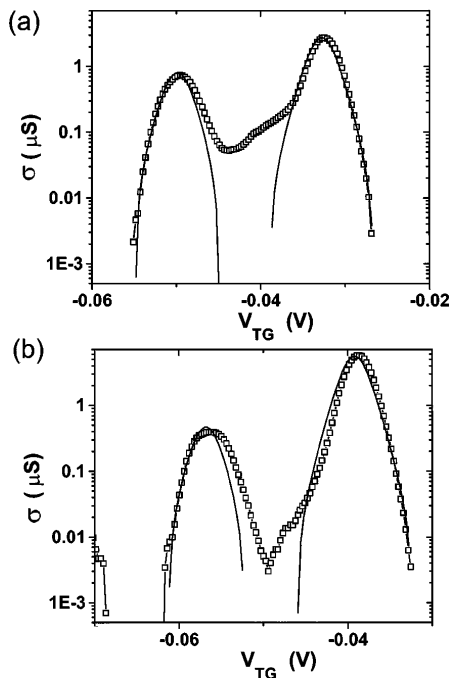


FIG. 3. (a) Magnified are the two conductance resonances at the crossing point. The additional—tunnel splitting—resonance is found in the left shoulder of the right peak. In (b) with a differently tuned back gate voltage the additional resonance shifts towards the valley between the two main peaks.

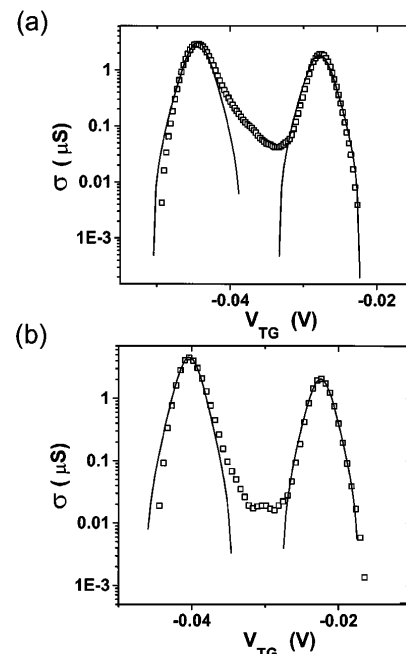


FIG. 4. As in (a) the two resonances are shown at stronger detuning: (a) Now in the tunnel splitted state appears in the right shoulder of the left peak. (b) The peaks in the shoulder are almost completely detuned.

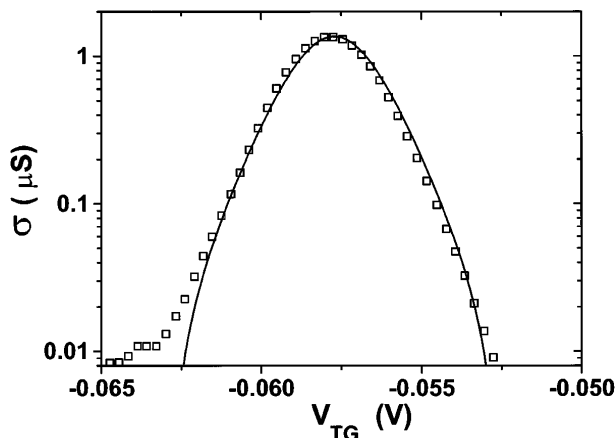


FIG. 5. Taking a resonance farther away from the crossing point, a common resonance shape without asymmetry is found. The fit is according to $\delta f_{FD}/\delta E$ as before.

the crossing point is another indication of the molecular coupling. The strong wave function overlap of the ground state results in electron transport. Since the discrete states are detuned in this regime, no tunnel splitting is found, and the peak structure remains symmetric.

In summary, we have shown that a coherent tunneling mechanism or molecular mode evolves in a coupled dot system. This coherent state is found as a tunnel splitting in addition to the Coulomb interaction in the charging diagram of the double dot. This state can be detuned within the charging diagram.

We gratefully acknowledge the support of Frank Stern in performing model calculations of the nanostructures. We thank Monika Riek and Frank Schartner for their technical support. This work was funded in part by the Bundesministerium für Bildung, Wissenschaft, Forschung und Technologie. D.P. gratefully acknowledges the

financial support by Grant No. Pf 256/2-1 of the Deutsche Forschungsgemeinschaft. R.H.B. thanks the Physics Department of Caltech for its hospitality.

*Present address: Sektion Physik Ludwig Maximilians Universität, Geschwister Scholl Platz 1, 80539 München, Germany.

Electronic address: robert.blick@physik.uni-muenchen.de

†Present address: Universität Hannover, Institut für Festkörperphysik, Appelstrasse 2, 30167 Hannover, Germany.

- [1] *Single Charge Tunneling*, edited by H. Grabert and M. Devoret, NATO ASI Vol. 294 (Plenum, New York, 1992).
- [2] W. Heitler and F. London, *Z. Phys.* **47**, 455 (1927).
- [3] F. Waugh *et al.*, *Phys. Rev. Lett.* **75**, 705 (1995); F. Hofmann *et al.*, *Phys. Rev. B* **51**, 13 872 (1995); R. Blick *et al.*, *Phys. Rev. B* **53**, 7899 (1996); D. Dixon *et al.*, *Phys. Rev. B* **53**, 12 625 (1996).
- [4] G. Klimeck, G. Cheng, and S. Datta, *Phys. Rev. B* **50**, 3126 (1994); C. A. Stafford and S. D. Sarma, *Phys. Rev. Lett.* **72**, 3590 (1994); G. Chen *et al.*, *Phys. Rev. B* **50**, 8035 (1994); C. Niu, L. J. Liu, and T. H. Lin, *Phys. Rev. B* **51**, 5130 (1995).
- [5] K. A. Matveev, L. I. Glazman, and H. U. Baranger, *Phys. Rev. B* **53**, 1034 (1996); **54**, 5637 (1996).
- [6] A self-consistent spatially resolved solution of the Poisson equation of the electrostatic potential landscape of the two dots with the gate configurations shown in Fig. 1 was performed. The calculations based on the algorithm developed by S. E. Laux, A. Kumar, and F. Stern [see also A. Kumar, S. E. Laux, and F. Stern, *Phys. Rev. B* **42**, 5166 (1990)].
- [7] J. Weis, R. J. Haug, K. von Klitzing, and K. Eberl, *Phys. Rev. Lett.* **71**, 4019 (1993).
- [8] For simplicity we assume the ground state to be symmetric, although from a general point of view, it might be antisymmetric.